ADVANCED SPATIO-TEMPORAL ANALYSIS OF SURFACE URBAN HEAT ISLAND INTENSITY IN THE MUMBAI METROPOLITAN REGION USING SURFACE IMPERVIOUSNESS, LAND USE- LAND COVER, AND LOCAL CLIMATE ZONES VIA GOOGLE EARTH ENGINE AND DEEP LEARNING (2003–2023)

PRIYANKA PURI*

Department of Geography, Miranda House, University of Delhi, Delhi-110007, India.
ORCID ID-0000-0002-8232-998X
**Corresponding author email: priyanka.puri@mirandahouse.ac.in*

Received: 3rd July 2025, **Accepted:** 23rd October 2025

ABSTRACT

Urbanisation significantly modifies land surfaces and amplifies local temperatures and heat stress. This study investigates Surface Urban Heat Island Intensity (SUHII) across the Mumbai Metropolitan Region (MMR) from 2003 to 2023 using Google Earth Engine (GEE) database and mapping. It integrates surface imperviousness from the Global Human Settlement Layer (GHSL), Land Use Land Cover (LULC), and the Local Climate Zone (LCZ) classification (2019) to explore spatial patterns in SUHII. Daily Land Surface Temperature (LST) data from MODIS was further analysed for details across 852 spatially sampled points, categorised by land cover types.

Findings reveal a consistent urban–rural SUHII of ~2 °C, with mean LSTs of 35.63 °C in urban and 33.67 °C in rural zones. Urban cores exhibit greater seasonal variability, with LSTs peaking above 51 °C in some areas. Auto Regressive Integrated Moving Average - ARIMA (2,1,1) time-series modelling indicates persistent warming trends, with 2023 pre-monsoon LSTs projected to exceed 44 °C in central MMR with an average of existing 51 °C in urban MMR and about 49 °C in rural MMR. A weak negative Pearson correlation (r = -0.19) between impervious surface intensity and SUHII suggests that built-up extent alone does not explain thermal intensity.

LCZ-based profiling shows that Compact High-Rise and Industrial zones have the highest LSTs, while vegetated zones maintain cooler profiles (<31 °C). Zones with >70 % impervious surfaces record disproportionately higher temperatures. Importantly, a review of existing studies shows that no published research has yet combined ARIMA forecasting with LOESS (Locally Estimated Scatterplot Smoothing) for MMR. This study uniquely combines remote sensing, statistical modelling (ARIMA, Pearson correlation), and urban climate zoning via cloud computing for the region. Deep Learning derived spatial datasets (GHSL, LCZ) enhance the spatial resolution of SUHII analysis. The results offer vital insights for climate-adaptive urban planning, emphasising zoning-based interventions, and landscape strategies to mitigate urban heat risks in expansive cities like Mumbai and its surroundings.

Keywords: Mumbai Metropolitan Region, Urban morphology, Surface imperviousness, ARIMA forecasting, Climate-resilient urban planning, Deep learning

INTRODUCTION

It is a well-established fact that urban centres are distinct from their surroundings in more than one way. One of the most visible manifestations is the temperature regime as urban systems absorb and emit radiated heat. The main sources are solar radiation and anthropogenic, with the latter dominating. Climate, weather, and diurnal variations also alter the Urban Heat Island Intensity (UHII) (Oke, 1995; Sachindra *et al*., 2016; Zhou & Chen, 2018). The effect of urbanisation and the nature of surfaces (Vujovic *et al*., 2021) is chiefly manifested in UHI, reflecting excessive heat generated by urban areas compared to surroundings (Cheval *et al*., 2023). Alongside UHI, 'cool islands' also occur in urban areas (Kim, 2007; Hulley, 2012; Qin, 2015; Rasul *et al*., 2017; Zhou & Chen, 2018; Budhiraja *et al*., 2019). Well documented and widely researched, Urban Heat Island (UHI) is a critical environmental concern of the 21st century arising from anthropogenic activities in urban regions globally (Rizwan *et al*., 2008; Sachindra *et al*., 2016; Zhou & Chen, 2018; Cheval *et al*., 2023). It is commonly measured through UHII, calculated as the spatially averaged temperature difference between urban and rural zones. The difference in mean maximum temperatures is referred to as the Mean Maximum Urban Heat Island Intensity (UHII) (Veena *et al*., 2020), with comparisons spanning daily to decadal scales.
UHIs have been categorised as follows (Stewart & Mills, 2021):

- Boundary Level UHI (BUHI) – Temperature above urban building heights.
- Canopy Level UHI (CUHI) – Temperature below the rooftop level, closely associated with SUHI.
- Surface UHI (SUHI) – Temperature of the physical urban surface.
- Substrate UHI (GUHI) – Sub-surface soil temperature variation.

So, SUHII indicates the strength of spatial observations of UHI at the surface. It is significant because the urban thermal signature begins at the surface and is shaped by land materials, geometry, and energy flows (Voogt & Oke, 2003; Lin *et al*., 2017; Zhou & Chen, 2018; Stewart & Mills, 2021). Expanding impervious surfaces—rooftops, pavements, asphalt roads—increase thermal storage and radiative emissions, intensifying SUHI. LST is a strong indicator of SUHI and SUHII, reflecting both natural and built surface characteristics (Lin *et al*., 2017; Rasul *et al*., 2017). Cities with dense construction and little vegetation show stronger UHI effects, particularly in summer (Lau *et al*., 2019; Morabito *et al*., 2021). LULC plays a central role in SUHI generation and seasonal variation. Land transformation from population growth, infrastructure expansion, and surface sealing links to elevated LST and deteriorating microclimates (Sarif *et al*., 2020). Hence, urban planning must integrate thermal maps for climate adaptation. LCZ framework by Stewart and Oke (2012) advanced UHI analysis by classifying urban and natural landscapes into 17 categories based on structure, cover, materials, and usage, enabling refined spatial differentiation of SUHI (Alexander & Mills, 2014; Zhou *et al*., 2022).

LCZs model urban morphology's effect on temperature beyond binary urban–rural contrasts, particularly useful in heterogeneous regions like Mumbai. The Mumbai Metropolitan Region (MMR), surrounding India's financial capital, shows extreme heterogeneity in LULC from dense built cores to vegetated coastal fringes and fragmented peri-urban zones. This complexity necessitates granular models integrating long-term LST with urban morphologies.

A miniscule of studies combine SUHII, LCZ, LULC, and imperviousness for MMR, forming the rationale for this research. GEE enables high-resolution LST extraction,

spatio-temporal analysis, and integration with impervious and LCZ datasets; supporting anomaly analysis, spatial sampling, ARIMA modelling, and geospatial correlation (Gorelick *et al*., 2017; Fang *et al*., 2024).

Deep learning models nonlinear relations between urban morphology and thermal characteristics (Zhao *et al*., 2022). Convolutional Neural Network (CNN) and hybrid models detect hotspots and classify LCZs (Bechtel *et al*., 2019). This work uses 852 spatially sampled points generated from GEE across the MMR for further detailed examination. These are stratified by LULC and LCZ classes to estimate SUHII over a two-decade period (2003–2023). The time-series analysis using ARIMA (2,1,1) reveals persistent thermal trends with a predicted rise of ~1.2 °C in dense commercial cores. Impervious surfaces >70 % (LCZs 1, 10) recorded LSTs > 50 °C (Tran *et al*., 2006; Nayak *et al*., 2023) in the current context with a weak Pearson correlation (r = - 0.19) between built-up index and SUHII. This underlines the complexity of urban heating as it is not just quantity of built-up but also the configuration, ventilation, material albedo (González, 2020) and green fractions that matter (Sharma *et al*., 2015). Thus, the study stands at the confluence of remote sensing, machine learning, climate modelling, and urban planning. By integrating SUHI analysis with LCZ and impervious surface dynamics, it enhances spatially targeted mitigation strategies like urban greening, reflective roofing, and zoning reforms.

Background of the Study and Literature Review

Urbanisation directly alters landscapes (Oke, 1995; Dihkan *et al.,* 2015; Derdouri *et al*., 2021). Historical UHI studies trace back to Luke Howard's 1818 work on London, noting temperature differences due to urbanisation (Stewart & Mills, 2021). Early research focused on microclimates, gaining momentum post-1945, and diversified after the 1970s with BUHI and CUHI studies (Stewart & Mills, 2021). SUHII also impacts quality of life and varies seasonally and topographically (Geletič *et al*., 2019; Hsu *et al.,* 2021). Building types, local climate, imperviousness, and vegetation cover influence UHI and SUHII (Pakarnseree *et al*., 2018; Zhou & Chen, 2018; Lu *et al*., 2020; Sarif *et al*., 2020; Morabito *et al*., 2021).

Remote sensing advancements further catalysed UHI research (Li *et al*., 2018; Stewart & Mills, 2021). Urbanisation and geography together affect temperature, as shown in Washington DC (Kim, 2007), Tehran (Haashemi *et al*., 2016), and Melbourne (Sachindra *et al*., 2016). It has enabled LULC and SUHI studies in Istanbul (Dihkan *et al*., 2015) and other cities (Gaur *et al*., 2018; Hou *et al*., 2021). SUHI has been studied for Indian cities such as Delhi, Bengaluru, Chennai, Kolkata, Nagpur, Mumbai, and Bhubaneswar using remote sensing (Thomas *et al*., 2014; Grover & Singh, 2015, 2016; Kikon *et al*., 2016; Swain *et al*., 2017; Dwivedi & Khire, 2018; Kotharkar & Bagade, 2018; Budhiraja *et al*., 2019; Dwivedi, 2019; Kumar & Mishra, 2019; Veena *et al.,* 2020; Gazi & Mondal, 2022; Shahfahad *et al*., 2022; Jain, 2023). SUHII, derived from LST, captures temperature variations directly observable via remote sensing (Voogt & Oke, 2003; Voogt, 2020). Increased built-up density and reduced vegetation drive SUHII and LCZs provides a framework to assess urban morphology's effect on temperature (Stewart & Oke, 2012; Alexander & Mills, 2014; Zhou & Chen, 2018; Sarif *et al*., 2020; Zhou *et al*., 2022). GEE enables LST and imperviousness analysis, supporting large-scale spatio-temporal assessments via databases such as LANDSAT and MODIS (Sharma *et al*., 2015; Gorelick *et al*., 2017; Morabito *et al*., 2021). Deep learning methods further enhance classification, prediction, and spatial pattern recognition (Bechtel *et al*., 2019; Zhao *et al*., 2022).

However, integrative studies combining SUHII, GEE-based analysis, LULC, imperviousness, and LCZ in India, especially for MMR are a rarity. MMRDA's spatial planning and development regulation increasingly rely on remote sensing, spatial modelling,

and AI-assisted analytics, while LCZ and LULC classifications inform urban thermal behaviour and heat mitigation strategies (Gorelick *et al*., 2017; MMRDA, 2021). This study addresses that gap by synthesising long-term LST trends with urban morphological classifications and surface characteristics.

Study Area

By the mid-nineteenth century, Greater Mumbai experienced intense overcrowding due to rapid population growth and industrial expansion. This led to land shortages, soaring property prices, and the growth of informal settlements. To reduce pressure on the city, a plan for a twin city across the harbour was proposed in 1958 and took shape in 1970 with the formation of the City and Industrial Development Corporation.

Regional development plans in India date back to the 1960s, emphasising region-oriented planning for metropolitan centres (Aayog, 2021). The Maharashtra Regional Town Planning Act (1966) introduced three-tier planning, followed by the 1970 Bombay Regional Plan. Thus, MMR Development Authority (MMRDA) was established in 1975 to refine these plans. In 1975, the MMRDA was established for regional planning (Sahu & Saizen, 2018). The new city, New Mumbai, was designed to accommodate 21 lakh people. To further support decentralisation, surrounding towns like Thane, Ulhasnagar, Bhiwandi, Khopoli, Kalyan, and Dombivali were also developed.

At present, the MMR spans approximately 6,355 km², including Mumbai City, Mumbai Suburban, and parts of Thane and Raigad districts (MMRDA, 2021, 2023). It is a part of the North Konkan region, features lowlands, hill ridges, rivers (Tansa, Patalganga), basaltic terrain, a long coastline, estuaries, and off-shore islands. MMR experiences a warm, humid climate with intense southwest monsoon rainfall from June to September, cooler winters, and hot pre and post-monsoon months.

Temperature extremes occur in January (minimum) and May (maximum). Winds range from 8 km/h (dry season) to 13 km/h (rainy season). Urbanisation has altered local climate, affecting wind patterns, rainfall, and temperature. Nearly 45 % of Maharashtra's population resides in MMR, with Mumbai's share declining from 76.89 % in 1971 to 54.56 % in 2011(MMRDA, 2023).

The region includes urban, semi-urban, and rural areas. Population density rose from 3,421 persons/km² (1991) to 5,361 persons/km² (2011), with high densities in Greater Mumbai, Ulhasnagar, Bhiwandi, and Thane. Built-up areas dominate land cover (MMRDA, 2023). Urban development is constrained by geography, with suburban railways and other transport modes supporting connectivity. About 1,000 villages exist, mainly clustered near urban centers, while eastern MMR remains agricultural. Pollution levels are high, and a lack of a unifying regional identity hampers data collection and planning (MMRDA, 2023).

MMR, one of India's largest and economically influential urban agglomerations, houses over 26 million people (Census of India, 2011; UN-Habitat, 2022) and contributes nearly 6 % to the national GDP (Shaw, 2012). Rapid growth has led to urban sprawl, wetland loss, green space reduction, and increased impervious surfaces (Bhatia *et al*., 2023). High-density housing with limited vegetation, including informal settlements, records elevated LST, especially in pre- and post-monsoon periods (Morabito *et al*., 2021). NRSC LULC data show Built-Up as the dominant land (MMRDA, 2023).

A region's physiographic diversity, coupled with unregulated expansion and informal housing, heightens vulnerability to flooding, heat stress, and air pollution (Dhar & Khirfan, 2017; Quang *et al*., 2022). Coastal influence and sea breeze moderates urban heat partially, while built-up interiors experience persistent SUHII from land-use change and

anthropogenic heat (Tran *et al*., 2006; Zhou *et al*., 2018). MMR includes Greater Mumbai and satellite towns (MMRDA, 2021). Ulhasnagar, Mumbai, and Bhiwandi are saturated, with Greater Mumbai holding 54.56 % of the population and the seven Corporations 32.7 %. Four—Thane, Kalyan-Dombivali, Vasai-Virar, and Navi Mumbai—are million-plus cities. Most residents work in the tertiary sector, though manufacturing has grown in metals, apparel, leather, machinery, and furniture (Sahu & Saizen, 2018; MMRDA, 2023). The location of study area along the city of Mumbai is depicted in Fig.1.1. Fig. 1.2.

Fig. 1.1: Location of Study Area

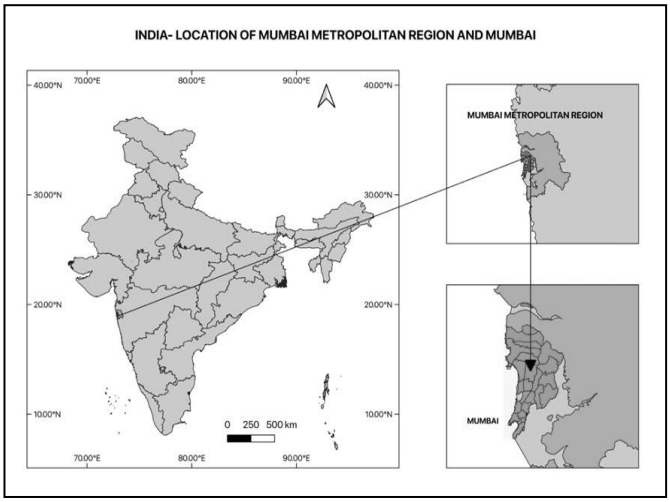

Source- Author, 2025

Growth is shifting outside Mumbai, constrained by geography. Suburban rail dominates, with expanding modes. About 1,000 villages exist, with clusters near centres. The eastern part of MMR remains largely agricultural. Pollution is high, awareness low, and unclear boundaries limit data (MMRDA, 2023).

Fig. 1.2: Study Area- Administrative Set Up

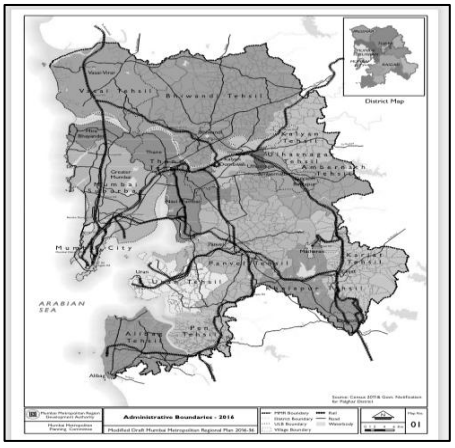

Source- MMRDA, 2023

Rapid growth drives ecological loss as wetland shrinkage, deforestation, and impervious expansion (Bhatia *et al*., 2023). Geographically- MMR's lowlands, estuaries, reclaimed marshes, and hills create flooding while heat stress and pollution risks are worsened by unregulated growth (Dhar & Khirfan, 2017; Quang *et al*., 2022). High-density, lesser vegetation and poor housing (especially informal settlements) experiences extreme LST in summer (Morabito *et al*., 2021). These complexities make MMR offer a vital case for studying urban form, land surface, and climate (Maral & Mukhopadhyay, 2015) and the challenges demand coordinated planning.

On the basis of the above observations, the following research questions have been designed:

i. Does there exist any heat island effect in MMR?
ii. If yes, then it is of what magnitude and intensity- SUHII?
iii. What postulates can be drawn for the LULC of the region and the resultant SUHII in space and time?

Hence, the MMR serves as a critical region for studying interactions between urban form, surface characteristics, and climate, where integrated spatio-temporal analyses using GEE and deep learning can guide climate-resilient urban planning.

MATERIALS AND METHODS

The study derives data from GEE databases. Land cover is derived from the European Space Agency (ESA) 'World Cover 10m v200' database, which provides a 2021 global land cover map at 10 m resolution from Sentinel-1 and Sentinel-2. It classifies 11 land cover types under the ESA World Cover project of the 5th Earth Observation Envelope Programme (EOEP-5). Physical landscape data is supplemented with NASA's SRTM Digital Elevation map derived at 30 m resolution. Surface imperviousness is analysed using the 'Tsinghua FROM-GLC Year of Change to Impervious Surface' database, which captures global changes in imperviousness from 1985–2018 at 30 m resolution. Changes from pervious to impervious surfaces are derived through supervised classification and temporal checks, with impervious surfaces defined as having more than 50 % imperviousness. The dataset spans 34 years, indexed as 34 and 1 for 1985 and 2018, respectively, and consistently reflects rural to urban transitions.

LCZs for 2018 are sourced from the 'Global LCZ dataset' by the Bochum Urban Climate Lab, representing urban landscapes via land cover and physical properties at a microscale. Designed to support urban heat island studies, the LCZ are calculated at 100 m pixels using multiple Earth observations and include 17 classes—10 built-up and 7 natural. Built-up categories include: compact high-rise, compact mid-rise, compact low-rise, open high-rise, open mid-rise, open low-rise, lightweight low-rise, large low-rise, sparsely built, and heavy industry. Natural classes include dense trees, scattered trees, bush/scrub, low plants, bare rock/paved, bare soil/sand, and water (Stewart & Oke, 2012). SUHII data is sourced from 'YCEO Surface Urban Heat Islands: Pixel-Level Annual Day-time and Night-time Intensity' and 'YCEO Surface Urban Heat Islands: Pixel-Level Composites of Yearly Summer and Winter Day-time and Night-time Intensity', providing averaged data for 2003–2018. These datasets are produced by the Yale Center for Earth Observation.

The statistical analysis in this study draws upon a robust combination of multi-source and multi-temporal geospatial datasets processed through the GEE platform and refined in

Python-based statistical environments. Primary focus is laid on deriving LST, SUHII, surface imperviousness, LULC, and LCZ for MMR. This is followed by a study of change in surface imperviousness to examine the conversion of the rural to the urban. The outcome is cross examined with the land cover/land use. Composites on the spatial extent of SUHIs are drawn for spatial average from 2003-2018. These averages are analysed as:

a. All day-time UHI
b. All night-time UHI
c. All summer day-time UHI
d. All summer night-time UHI
e. All winter day-time UHI
f. All winter night-time UHI

These datasets are processed in QGIS 3.26 software. The methodology based on spatial derivations is mathematically analysed as described further.

The ARIMA model is a widely used statistical technique for time-series forecasting, especially effective for modelling climate variables with linear trends and seasonality. The general form of an ARIMA model is ARIMA (p, d, q), where *p* is the order of autoregression, *d* the degree of differencing, and *q* the order of the moving average. The standard equation is:

Yt=c+ϕ1Yt−1+⋯+ϕpYt−p+θ1ϵt−1+⋯+θqϵt−q+ϵtY_t = c + \phi_1 Y_{t-1} + \cdots + \phi_p Y_{t-p} + \theta_1 \epsilon_{t-1} + \cdots + \theta_q \epsilon_{t-q} + \epsilon_tYt =c+ϕ1Yt−1+⋯+ϕpYt−p+θ1ϵt−1+⋯+θqϵt−q+ϵt

where, YtY_tYt is the differenced series (if d>0d > 0d>0), ϕ\phiϕ and θ\thetaθ are AR and MA coefficients, and ϵt\epsilon_tϵt is white noise. ARIMA (2,1,1) is a forecasting model that applies first-order differencing to non-stationary data, with two autoregressive and one moving average terms. It captures recent trends and residual shocks, making it useful in environmental and climate modelling (Box *et al*., 2015). ARIMA forecasting extrapolates future values based on past trends, offering practical utility in temperature or rainfall projection studies (Box *et al*., 2015).

LOESS is a non-parametric regression method that fits simple models to localised subsets of data for capturing non-linear patterns (Cleveland *et al*., 1990). The LOESS curve at point *x* is obtained by weighted least squares, emphasising nearby points using a kernel function. Unlike ARIMA, LOESS does not assume a global model form and is highly effective in detecting seasonal cycles and smooth climatic transitions (Cleveland *et al*., 1990). Together, ARIMA and LOESS serve as complementary tools for understanding and forecasting climatic variability.

A specific focus also remains on the rural and urban distinction of the landscape. This is attempted through a spatial set of 852 points derived as samples from GEE from the rural and urban areas identified as per the LULC of the region. An attempt is made to study the geography, land over, land use, and surface imperviousness to derive conclusions regarding the SUHI and SUHII for the region. It is expected to provide a further more detailed outcome to the study which is difficult to obtain in the field.

RESULTS

According to MMRDA, satellite-based information from 2007 indicated that agriculture dominated land cover at 31 %, followed by scrub/grassland and wasteland (MMRDA, 2023). Forests accounted for 19 %, built-up 16 %, coastal features and wetlands 7 %, water bodies 4 %, and industry 2 % (MMRDA, 2023). By 2016, built-up area reached 697.01 sq. km, including developed rural and urban uses, transport networks, recreational spaces, quarries, and suburban railways. Although both rural and urban in character; urban built-up contributes most to SUHI, with Mumbai city recording the maximum share. However, rural areas have also grown rapidly.

The basic observation on the existence of an exceptional temperature regime in MMR is more pertinent in the urban area of Mumbai city and immediate suburbs year-round. This examination is an outcome of the study of overall yearly day-time and night-time SUHII, followed by a seasonal analysis of summer and winter day and night-time SUHIIs as can be seen in Fig. 2.1.-2.6.

The derivations indicated some common regions for SUHI and hence, SUHII. These can be identified as:

a. Mumbai city, Mumbai suburb, extending northeast to Thane, Bhiwandi and Kalyan-Dombivali in a contiguous zone. Interestingly, this region includes urban built-up in the north-western part, but its continuation in the east and middle of MMR occurs not only in the ridge zone but also in tree cover and cultivated region as supported by Fig. 3. and 5.
b. Extreme western part of Vasai
c. Uran Tehsil
d. Pen Tehsil
e. Part of Panvel Tehsil
f. Southern part of Khalapur Tehsil (for location refer Fig. 1.2.; for LULC refer Fig. 5.)

While much information exists on MMR's housing stock, its basic nature cannot be derived from field observations. LCZs proves useful here, revealing diverse morphologies created by occupancies, with open low-rise dominating as can be seen in Fig. 6 and 7. Slums account for slightly more than one-third of MMR housing and the findings well relate to the fact.

The detailed findings are as follows:

SEASONAL AND GEOGRAPHICAL TRENDS IN SUHI/SUHII (2003-2018)-

All day and night-time SUHII from 2003–2018 indicate a differential trend across the regions of the study area for day and night. Regions a-f in Fig. 2.1. correspond to the ones described in the results section. Region 'a' shows that SUHII day- time values trend towards a decline but night-time averages show the highest values for MMR as observed in Fig. 2.1. and 2.2.

Fig. 2.1: MMR- All Day- time SUHII

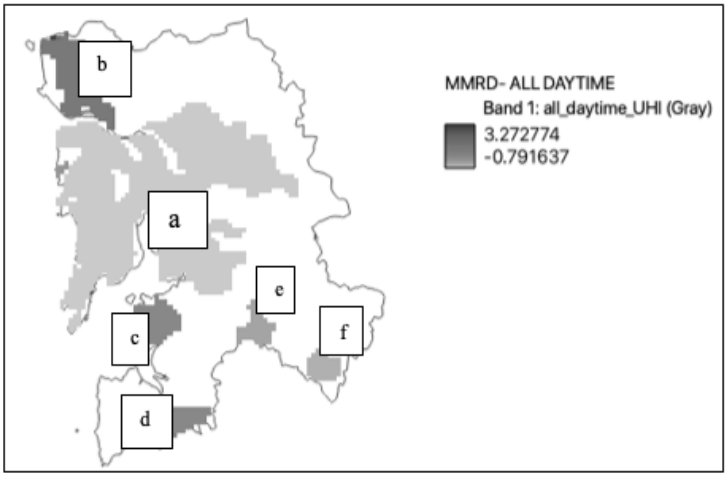

Fig. 2.2: MMR-All Night-time SUHII

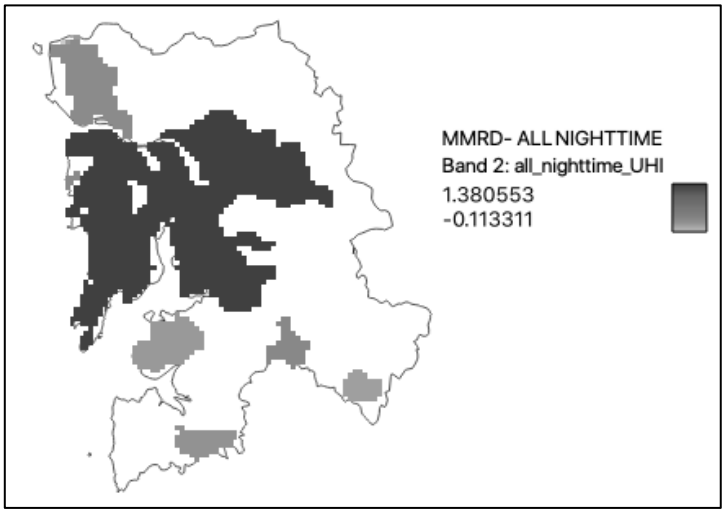

Fig. 2.3. and 2.4. provide further detail the seasonal trends.

Fig. 2.3: MMR- All Summer Day-time SUHII

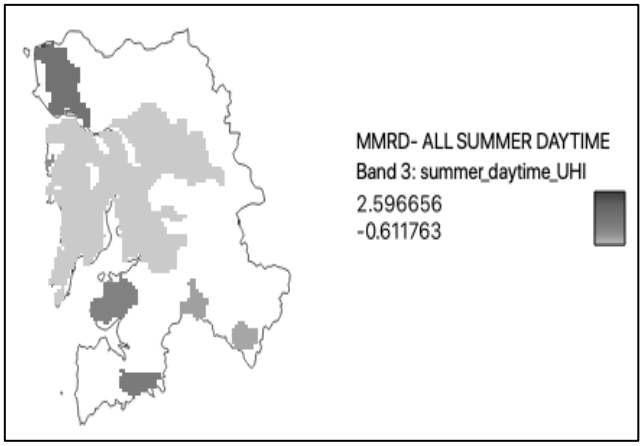

Fig. 2.4: MMR- All Summer Night-time SUHII

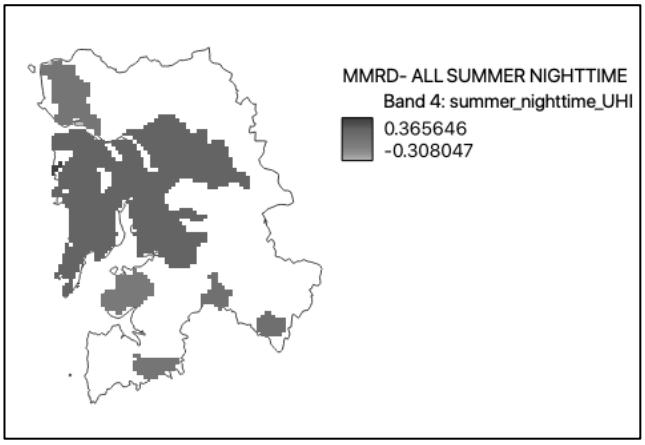

Fig. 2.5: MMR- All Winter Day-time SUHII

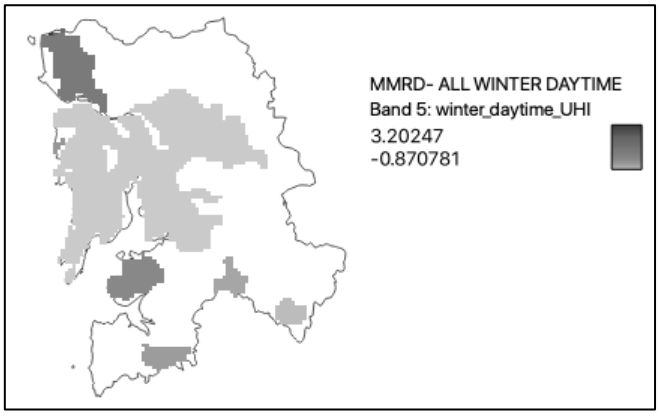

Fig. 2.6: MMR- All Winter Night-time SUHII

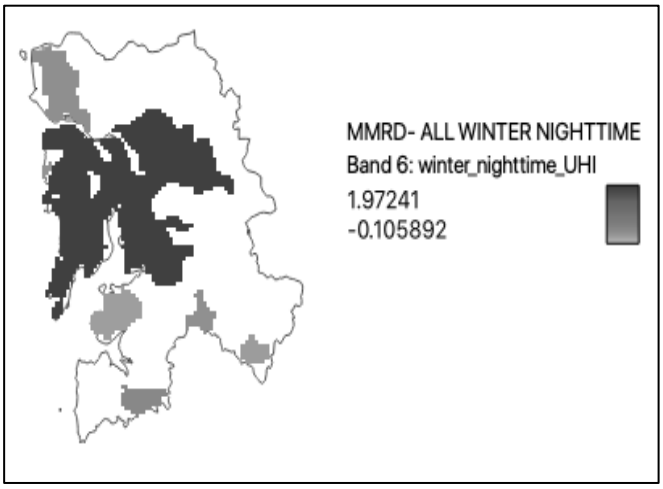

All data is in °C

Source For Fig. 2.1.-2.6. - Author, 2025 from YCEO Surface Urban Heat Islands database from GEE

The maps depict Surface Urban Heat Island (SUHI) intensity across the Mumbai Metropolitan Region (MMR) for day and night-time. Daytime values range from –0.79°C to 3.27°C, indicating moderate heating concentrated over central and northern MMR (zones a, b, and e), where dense built-up and industrial surfaces dominate. Cooler zones (d and f) correspond to vegetated or coastal areas with stronger evaporative cooling. At night, the SUHI range narrows to –0.11°C to 1.38°C, yet the spatial extent of warming expands, especially across the western and inner metropolitan zones—revealing high heat retention and limited nocturnal cooling. The weaker negative values at night suggest persistent residual heat storage in impervious materials.

The seasonal variation of night-time Surface Urban Heat Island Intensity (SUHII) across the Mumbai Metropolitan Region (MMR) reveals the strong influence of maritime climate and seasonal dynamics. Dense urban cores retain heat due to impervious materials, anthropogenic heat emissions, and restricted longwave radiation loss, while surrounding rural and vegetated zones cool rapidly under clear, calm skies, creating a pronounced thermal gradient. During winter night- time, SUHII values range from −0.10 °C to 1.97 °C, indicating a stronger and spatially extensive nocturnal heat island. In contrast, the summer night-time SUHII weakens notably, ranging from −0.30 °C to 0.36 °C. This reduction reflects enhanced atmospheric mixing and stronger sea-breeze circulation that facilitate heat dispersion and diminish night-time temperature differences.

The contrasting winter–summer relationship highlights that SUHI effects in MMR are most pronounced under stable winter conditions, when radiative cooling dominates, and weakest during humid, convective summer nights. This seasonal reversal underscores the combined roles of maritime influence, atmospheric turbulence, and surface energy balance in shaping urban thermal regimes within Mumbai's unique coastal environment. Overall, the shift from a wider daytime range to a narrower but spatially stronger night-time SUHI reflects the cumulative effect of urban morphology, surface properties, and coastal modulation on MMR's diurnal thermal regime.

These results can further detailed as follows:

A - SUHI/SUHII, geography and LULC- The geography of the region as indicated earlier, is marked by low land region and ridges. This is reflected in Fig. 3. and 4. The Digital Elevation Model (DEM) shows the range of elevation with lowland and ridge topography. When examined with SUHII, it is clear that the lowlands have a concentration of SUHIs observed for the region. This is also coinciding with the fact that these spaces are under habitation; strengthening the role of human influence.

Fig. 3: MMR- Geographic Features

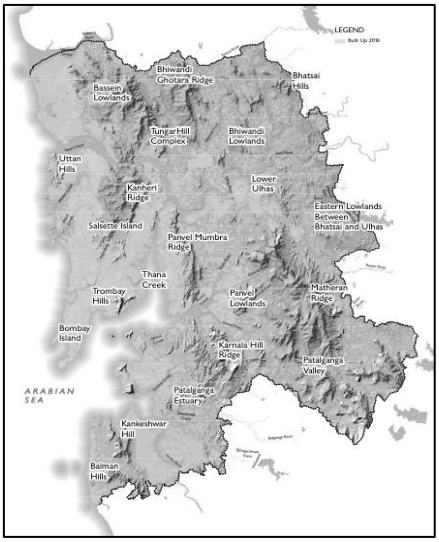

Source- MMRDA, 2023

Fig. 4: MMR- DEM

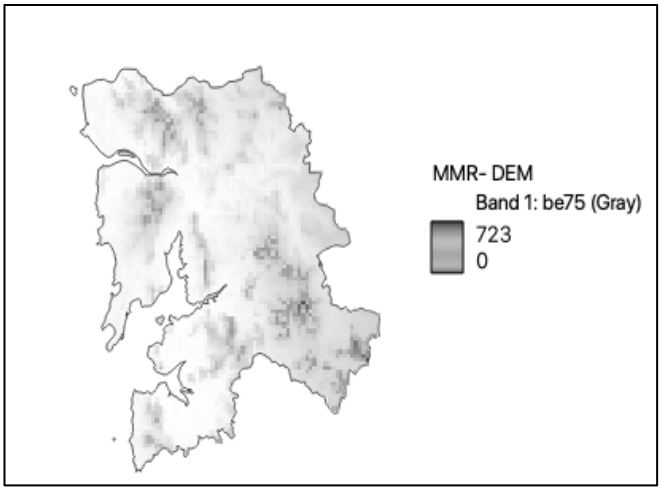

Source- Author, 2025, from NASA SRTM Digital Elevation 30m from GEE

So, basically it is the habitable portion of MMR which is exhibiting the existence of SUHI and resultant SUHII. However, neither geography nor LULC seem to dictate the intensity of the phenomena.

B - SUHI, SUHII and LULC- As is visible in Fig. 5., maximum SUHI and SUHII is visible in the Built-up area. LULC is attempted for 2021. Region 'a' and 'b' have maximum SUHII. Both indicate the dominance of built up area, while region 'c' and 'd' shows a mix of both the built-up area and natural features. However, regions 'e' and 'f' do not necessarily show the dominance of built- up area but an invariable SUHII is recorded (Refer Fig. 1.2. and 2.1.- 2.6.).

Fig. 5: MMR- Land Use/Land Cover

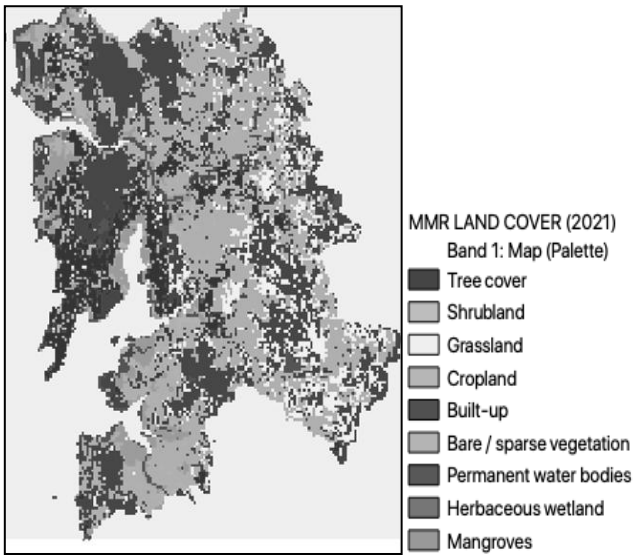

Source- Author, 2023; derived from ESA World Cover Database (2021) from GEE

C - SUHI/SUHII AND SURFACE IMPERVIOUSNESS- Surface imperviousness analysis in Fig.6. is derived from 1985 to 2018 indicated as 34-1 years in the index. From this, it is clearly established that surface impervious coincides with SUHI in its geographical extent and consequently in generating SUHII. All regions exhibiting SUHI also indicate older and newer surface imperviousness. However, older surface imperviousness regions exhibit a higher lower day-time SUHII, particularly Mumbai city region and immediate surroundings.

LOCAL CLIMATE ZONES AND SUHI/SUHII- The LCZ of the region is diverse as can be seen in Fig.7. Here, two categories seem to dominate the landscape. These are open low- rise and scattered trees. SUHI coincides basically with the LCZ of open low-rise in Regions 'a','b', 'c', 'e', and 'f'. The low-rise is also marked with compact midrise particularly in Region 'a' (Refer Fig. 2.1.- 2.6.).

Fig. 6: MMR- Change in Surface- Pervious to Impervious (1985-2018)

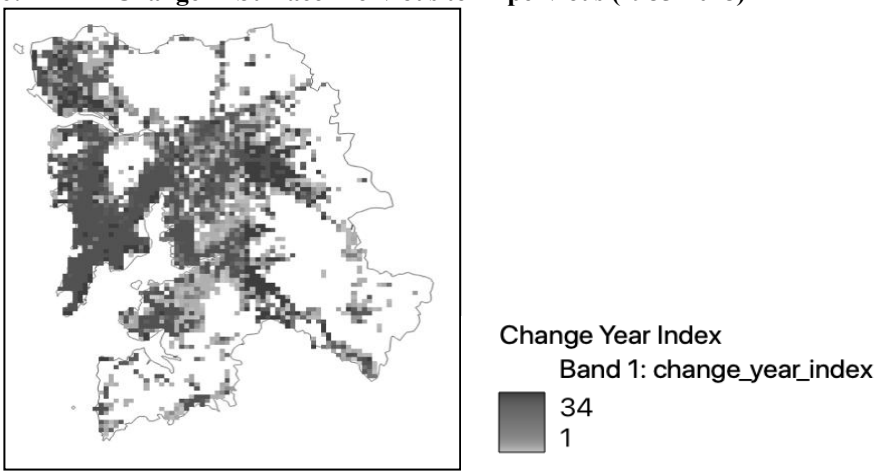

Source- Author, 2025; derived from Tsinghua From-GLC Year of Change to Impervious Surface database from GEE

Fig. 7: MMR- Local Climate Zones (2018)

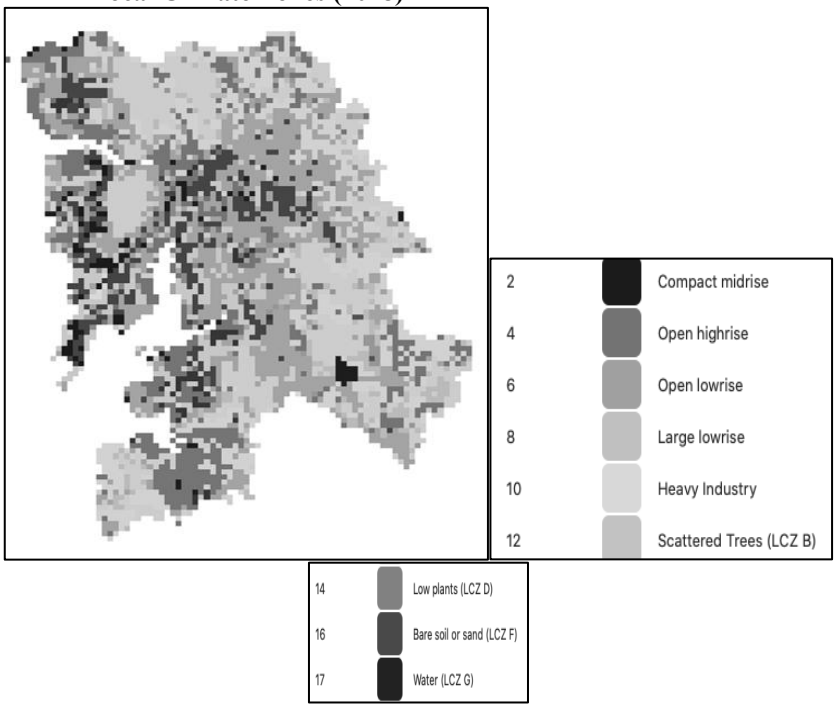

Source- Author, 2025; derived from Global map of Local Climate Zones, Bochum Urban Climate Lab database from GEE

D - SUHII AND MATHEMATICAL INTERPRETATIONS- SUHII trends are interpreted for further details. In Fig. 8., the time series graph presents SUHII from 2003–2023 with a 12-period rolling mean to provide insights into short-term variations and long-term trends. SUHII, examined as the temperature difference as per built-up, is influenced by land cover, anthropogenic heat, and seasonal climate. Fig. 8. plot shows a distinct seasonal pattern, with SUHII peaking in summer due to high solar radiation and reduced vegetation. These recurring peaks and troughs highlight the cyclical nature of the phenomena, driven by climatic seasonality.

The 12-month rolling mean smooths fluctuations and emphasises broader trends. Overall, the rolling average suggests relative stability in long-term SUHII. While some years show slight increases or decreases, there is no clear trend, indicating that the UHI effect has remained largely consistent while SUHII showing rises and dips beyond the range of UHI. This is an important output and is a strong indicator of regional influences.

Fig. 8: MMR- Basic Statistical Trends in SUHII

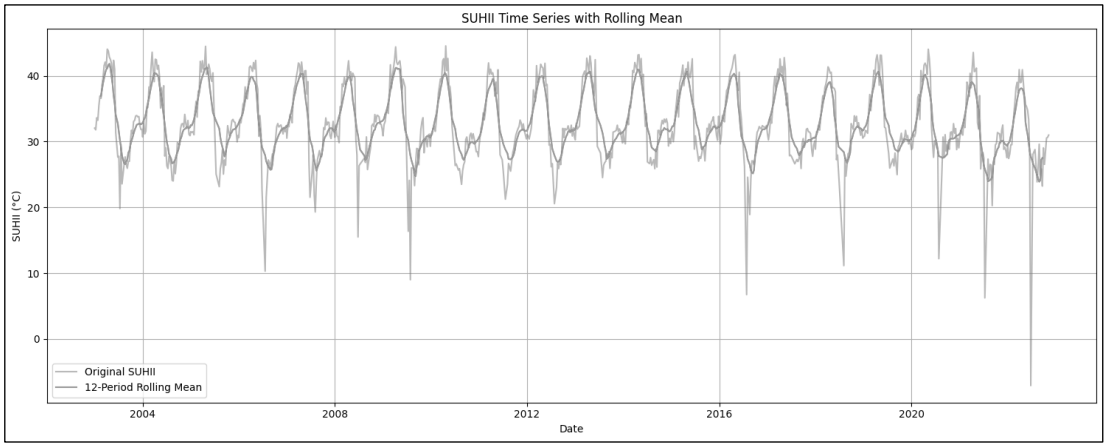

Source- Author, 2025

Some years do exhibit sudden dips in SUHII values—especially around 2006, 2009, and 2021. These anomalies could be attributed to probable data gaps, extreme weather events (e.g., heavy monsoons or cyclones), or possibly urban interventions like increased green cover or changes in land use patterns which are somehow less likely. In summary, the SUHII time series demonstrates strong seasonal variability with stable long-term behaviour. Further statistical analysis could help confirm the presence or absence of subtle trends and investigate the causes behind abnormal fluctuations observed in specific years, specifically in a spatial aspect.

Fig. 9: MMR- LOESS Analysis of SUHII

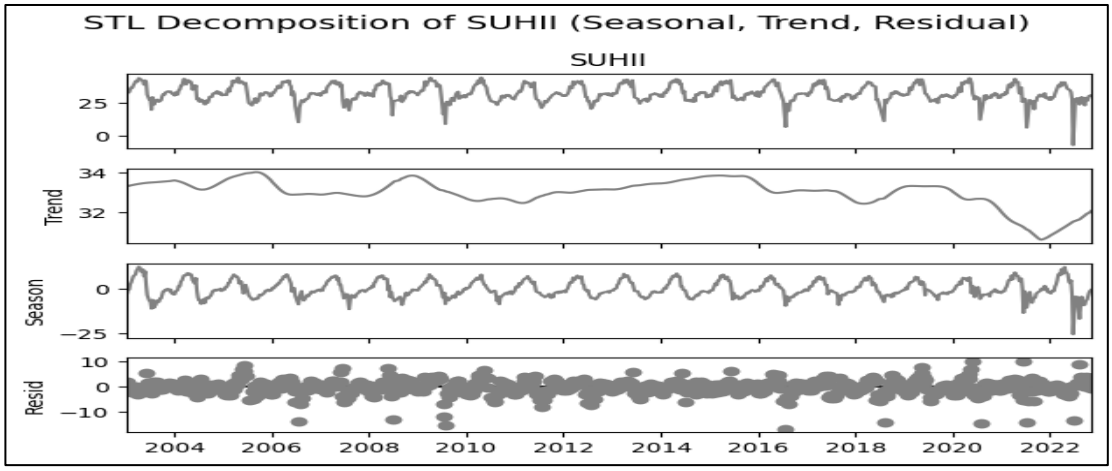

Source- Author, 2025

The Seasonal-Trend decomposition using LOESS (STL) decomposition of SUHII in Fig.9. reveals distinct temporal characteristics. The trend shows a relatively stable, slightly fluctuating increase until 2018, followed by a distinct decline. The seasonal component displays strong, consistent annual cycles, confirming dominant seasonal influences on urban heat. Residuals are scattered with occasional extremes, reflecting episodic anomalies like abrupt cooling or heating. Post 2020 indicates a sudden shift in the pattern.

Overall, SUHII is shaped primarily by seasonal patterns, with moderate long-term shifts and localised irregularities. This decomposition clarifies how much SUHII variability stems from natural seasonality versus long-term structural urban–climatic changes.

Fig. 10: MMR SUHII- ARIMA Forecast

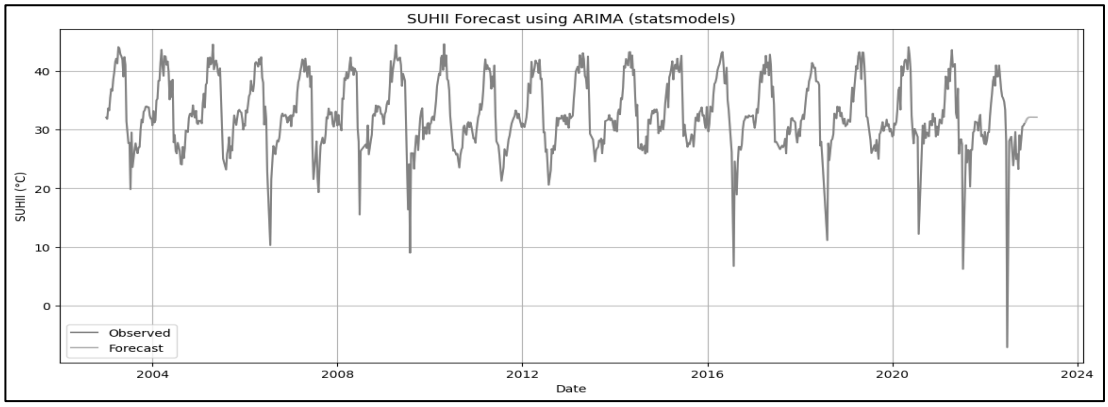

Source- Author, 2025

The ARIMA-based forecast of SUHII when cross examined with LOESS in Fig.10. shows that the model effectively captures observed seasonal and trend components from historical

data spanning 2003 to 2022. The forecast extends into early 2023, closely following recent patterns. This indicates that ARIMA performs well for short-term forecasting, especially in replicating seasonal peaks and troughs. However, occasional deviations suggest that while robust, it may not fully account for sudden anomalies or outliers.

ARIMA provides a reliable approximation for near-future SUHII behaviour based on historical trends. In addition to capturing seasonal cycles, it demonstrates strong performance in handling non-stationary time series with regular periodicity for the region. The consistent alignment of forecasted values with observed data highlights the past SUHII patterns into the future. However, extreme values, possibly linked to unusual climatic events or data irregularities in the MMR don't seem to deviate the LOESS trends also which needs to be explored in further detail.

Fig. 11: MMR- Correlation Between Built- Up Surface and SUHII

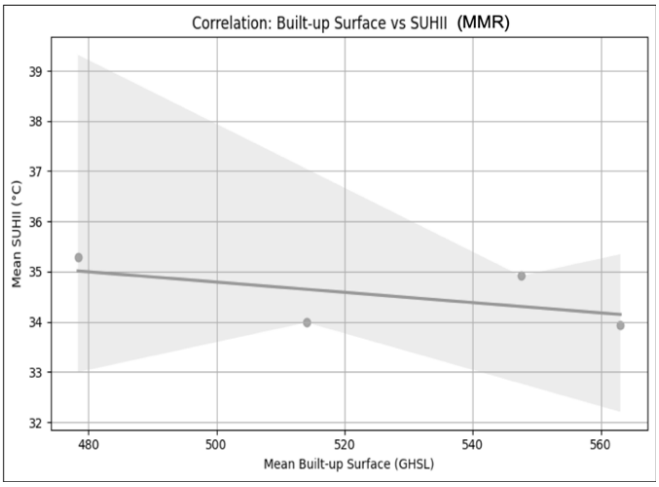

Source- Author, 2025

The scatter plot in Fig.11. illustrates the correlation between mean built-up surface (sourced from GHSL) and mean SUHII for the MMR. Each point represents a temporal average or spatial unit, while the fitted regression line with shaded confidence interval shows the linear trend and its uncertainty. Interestingly, the trend line reveals a slight negative correlation, suggesting that as built-up surface increases, SUHII decreases marginally. This appears counterintuitive, as urban expansion is typically associated with higher SUHII due to heat-retaining materials and reduced vegetation. This is also supported partly by day- time SUHII as is seen in Fig.2.1.-2.6.

A distinct spatial sampling through GEE is next attempted to detail findings at a finer spatial level. The findings are highlighted below.

SPATIAL SAMPLING AND FINDINGS- In this study, a total of 852 spatial sampling points were generated to capture the spatio-temporal variation in SUHII across the Mumbai Metropolitan Region (MMR) from 2003 to 2023. The points were systematically derived using stratified random sampling through GEE, ensuring representative coverage across diverse LULC and LCZ categories as per the regional classification into rural and urban. The criterion of classification of these points can be seen in Table1. and Fig.12.

Table 1: MMR- Region Classification Criteria for Sampled Points

Type	Imperviousness (%)	LCZ Types
Urban	> 50%	LCZ 1–10 (Built-up zones)
Rural	< 20%	LCZ A–G (Natural zones)

Source- Author, 2025 from RUBCLIM dataset from GEE

Fig. 12: MMR- Sampling Locations Derived from GEE

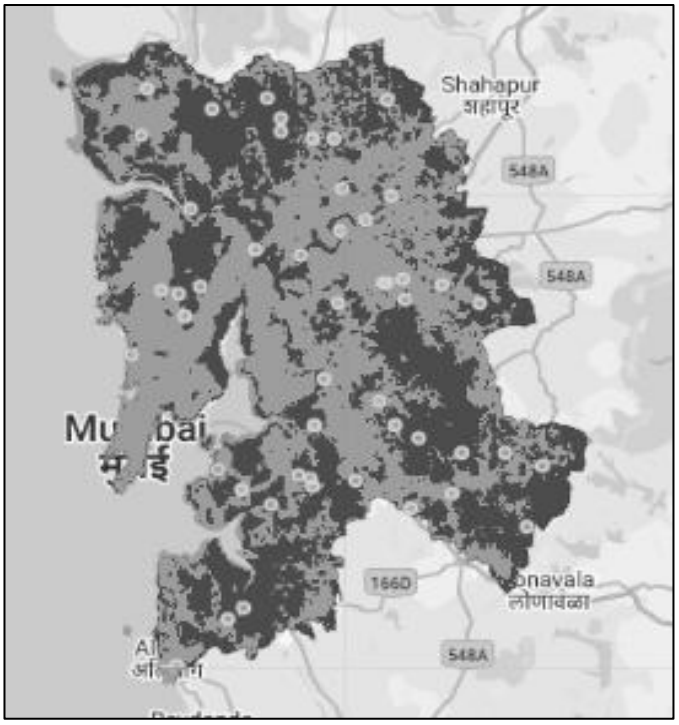

Source- Author, 2025 from RUBCLIM dataset (Light shade shows urban areas and darker indicates rural areas) from GEE

Although the companion Bochum raster did not explicitly label LCZ 1, morphology-informed attributes within GEE identified compact high-rise samples. These points were retained to represent thermally extreme urban forms documented in ground reality. Consequently, LCZ 1 results reflect point-level strata rather than continuous raster patches. The sampling aimed to balance representation across urban, peri-urban, and rural zones, while considering factors like surface imperviousness and urban morphology. Refer Fig.7. for details.

Each point was linked to corresponding LST values from MODIS data through GEE interface, and temporal profiles were used to compute SUHII time series. The points served as statistically robust units for trend detection, forecasting, and correlation analysis. Their distribution across zones established a strong basis for spatial modelling of thermal variation,

helping identify SUHII hotspots in MMR's core and cooler zones in its peripheries. Average urban and rural temperatures as generated for these regions are given in Table 2.

Table 2: MMR- Urban and Rural Mean LST- 2003-2023

Region	Mean LST (°C)	Std. Dev	Min (°C)	Max (°C)
Urban	**35.63**	5.44	6.05	51.11
Rural	**33.67**	5.19	-7.07	49.13

Source- Author, 2025

The negative minimum LST value (−7.07 °C) observed in rural zones does not indicate an actual freezing surface temperature but likely results from data artefacts or terrain-induced variations. Such values can arise from residual cloud contamination, high-altitude forested areas, or mixed pixels containing water and vegetation with lower radiant temperatures. In contrast, the urban minimum temperature (6.05 °C) remains positive due to the heat retention capacity of impervious surfaces. Therefore, the negative LST in rural regions represents spatial or seasonal heterogeneity rather than true cold extremes, while overall thermal contrast still indicates the presence of a SUHI effect, reflecting temporal dynamics influenced by elevation, coastal regulation, and seasonal monsoon cooling.

Fig. 13: MMR- Mean LST of Sampled Points

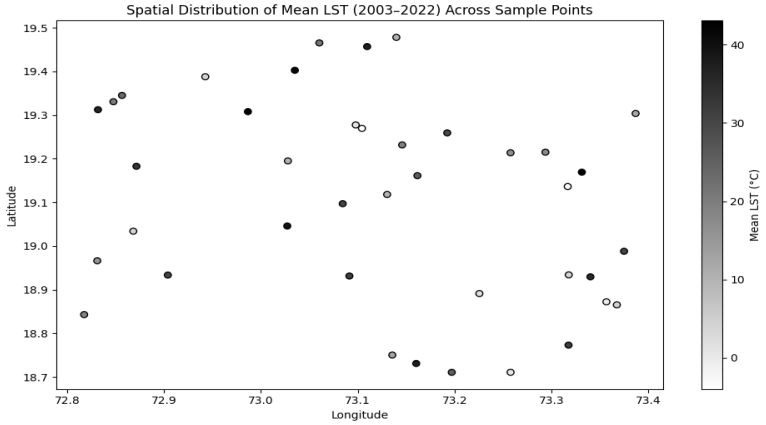

Source- Author, 2025

The scatter plot in Fig.13. visualises mean LST across locations between 2003 and 2022, using reversed colour shading to highlight temperature variation—lighter shades indicate cooler areas, while darker shades indicate warmer ones. Each point represents a geographic location, with latitude on the y-axis and longitude on the x-axis. The colour scale shows spatial variation in surface temperature, with most points clustered within a moderate LST range. A few isolated locations display higher LST values, suggesting urban heat islands or areas with less vegetation and more impervious surfaces. Conversely, darker-coloured points represent warmer regions. Overall, the plot highlights spatial heterogeneity in long-term LST

patterns and serves as a basis for linking land cover, elevation, or urban form with temperature dynamics. Fig.14. illustrates fluctuations in rural and urban temperatures.

Fig. 14: MMR- Urban and Rural Mean LST

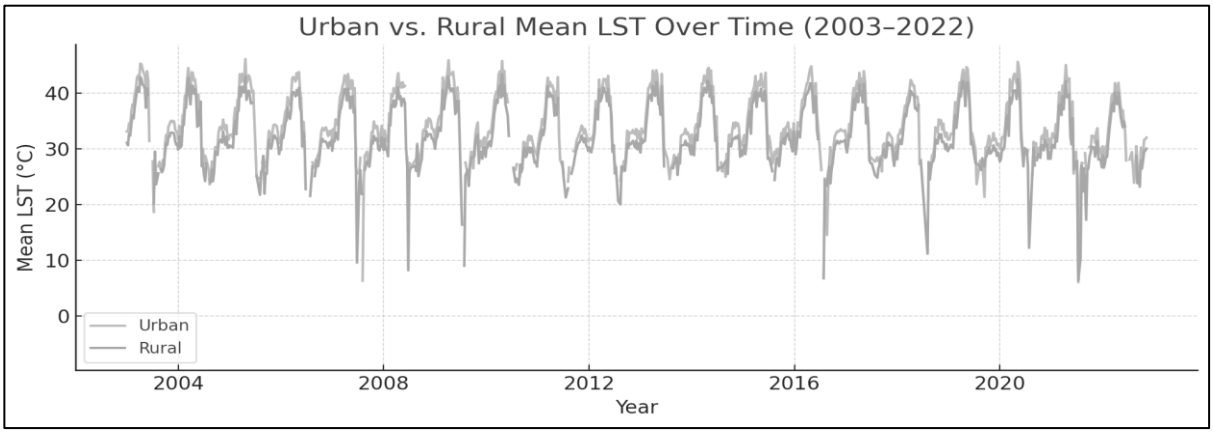

Source- Author, 2025

Fig. 15: MMR- Mapping of LST of Sampled Points

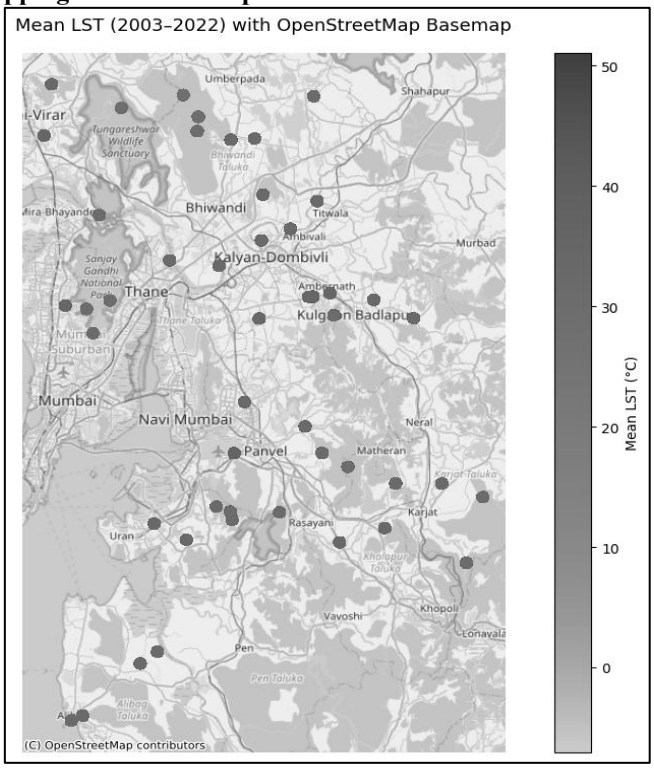

Source- Author, 2025

The spatial depiction of this map is in Fig.15. Geographic coordinates are plotted over spatial locations referenced from OpenStreetMap (OSM), which provides freely accessible, community-generated vector data on roads, buildings, land use, and urban infrastructure, serving as a reliable base for spatial referencing and urban analysis. The spatial graph of mean LST (2003–2022), overlaid on an OSM base map, reveals distinct thermal patterns across MMR. Higher LST values (40–50 °C) are concentrated in core urban zones like Mumbai, Thane, and Navi Mumbai—areas with dense built-up land cover and impervious surfaces. In contrast, peripheral regions such as Karjat, Panvel, and eastern and north-eastern boundaries exhibit much lower LSTs (<20 °C), reflecting cooling effects of vegetation, water bodies, and lower urban density.

The visual gradient confirms a classic UHI effect, with intense heat retention in compact and industrial LCZ. The spatial variation also aligns with land cover classifications, indicating that LST is shaped not only by built-up density but also by geographic location and local morphology.

DISCUSSIONS

This study offers a comprehensive and high-resolution spatio-temporal assessment of SUHII in the MMR across a two-decade timeline (2003–2023), providing novel insights into the dynamics of urban thermal environments in a rapidly expanding megacity. Leveraging GEE, MODIS-derived daily LST, and advanced urban form classifications such as LCZ, the research introduces a multidimensional approach to evaluating heat patterns in heterogeneous urban settings. The results confirm a persistent urban–rural LST differential (~2 °C), with urban cores experiencing intensified thermal stress and seasonal extremes exceeding 51 °C. These thermal peaks represent potential public health and environmental threats in a region already vulnerable to heatwaves and infrastructural stress (Sharma *et al*., 2015; Su *et al*., 2022).

What sets this study apart is its methodological innovation and data integration framework, which combines remote sensing, spatial sampling, statistical modelling, and urban climatic classification in a cloud-based environment. The LCZ layers were obtained from the RUBCLIM Global LCZ dataset (Bechtel *et al*., 2019) available on Google Earth Engine, representing the urban morphology of approximately 2018. The dataset provides globally consistent LCZ classification at 100 m resolution, which was subsequently clipped to the Mumbai Metropolitan Region (MMR) and integrated with MODIS-derived temperature and surface imperviousness data for the 2003–2023 analysis.

With 852 spatial points sampled across the MMR, the study ensures statistical representation and landscape diversity, incorporating urban, peri-urban, coastal, vegetated, and industrial zones. These points were contextualised using GHSL impervious surface data and LCZ classification (2019), which provided a morphology-based lens into urban form—something rarely used in Indian UHI studies (Bechtel *et al*., 2019). A review of UHI literature reveals that no prior study in the Indian context—and particularly in MMR—has integrated LCZ-based classification with statistical forecasting and high-frequency daily LST time series, making this research unique. It is also positioned to address a crucial knowledge gap (Zhou *et al*., 2021).

The use of LCZs, a framework developed for urban climatology that classifies cities based on surface cover, building geometry, and functional use, enables a more nuanced understanding of thermal behaviour (Stewart & Oke, 2012). These findings affirm that built-up morphology and not merely imperviousness, plays a decisive role in heat intensity. The weak negative Pearson correlation ($r = -0.19$) between built-up density and SUHII

further substantiates that urbanisation extent alone is insufficient to explain thermal anomalies. Instead, material reflectivity, ventilation potential, surface texture, and spatial composition are equally, if not more, influential in determining local heat regimes (Zhou & Chen, 2018; Qin *et al*., 2022). Urban heat islands usually show higher temperatures in built-up areas, but in desert cities this pattern can invert because bare soil heats more than urban materials (Lazzarini *et al*., 2013). This shows that SUHI behaviour depends strongly on local climate and land cover context (Lazzarini *et al*., 2013) and consequently SUHII.

A major novelty lies in the application of ARIMA (2,1,1) modelling to forecast LST trends. While time-series analysis has been used in climatology and hydrology, its application to SUHII forecasting in Indian contexts is rare. Most prior studies focus on trend estimation using linear regression or non-parametric methods, often at seasonal intervals (Gaur *et al*., 2018). This study advances the discourse by implementing a pixel-level forecast model projecting pre-monsoon LSTs exceeding 44 °C in central MMR for 2023. No other study, as seen in literature, has employed ARIMA forecasting alongside LCZ and impervious surface data to analyse urban heat in the MMR. This predictive component is essential for urban heat risk planning, heatwave preparedness, and infrastructure resilience (Kusak & Kucukali, 2024).

Moreover, the use of daily MODIS LST data allows for unprecedented temporal granularity. Indian UHI studies traditionally rely on snapshot analyses from Landsat or ASTER, constrained by revisit cycles and cloud cover. This work capitalises on MODIS's daily coverage to build continuous time-series, offering better characterisation of thermal extremes, intra-seasonal variability, and inter-annual trends. It also validates assumptions about seasonal heat build-up and dissipation in different land-use contexts (Dwivedi & Khire, 2018). A survey of existing studies confirms the absence of such daily-scale UHI tracking over extended periods in Indian megacities, especially Mumbai (Ren *et al*., 2023). Alves *et al*. (2020) demonstrated that SUHI in medium-sized cities shows clear spatial heterogeneity and seasonal variability. Their findings highlight that SUHI is not uniform but shifts with land cover and urban morphology (Alves *et al*., 2020).

Additionally, using cloud computing via GEE makes this study replicable, scalable, and efficient. GEE enabled rapid processing of large LST datasets over 20 years and seamless integration of global datasets like GHSL and LCZ. Its computational efficiency supported complex analyses—such as spatial sampling, temporal smoothing, and ARIMA modelling—within an open-access platform, crucial for democratizing urban climate research in data-scarce contexts like India (Gorelick *et al*., 2017). Beyond methodology, this study's broader significance lies in its implications for urban sustainability, resilience, and climate justice.

SUHII disproportionately affects marginalised populations residing in thermally stressed zones with limited cooling infrastructure (Kotharkar & Bagade, 2018). Zonal insights into compact high-rise and industrial areas resonate with global findings that highlight morphology and material use as critical for heat mitigation (Santamouris, 2020). By showing the inadequacy of imperviousness-based metrics alone, the research aligns with calls for morphology-sensitive UHI assessments (Martilli *et al*., 2020).

This work also contributes to climate adaptation discourse by offering spatially explicit evidence to guide nature-based solutions like urban greening and blue infrastructure integration (Kabisch *et al*., 2017). The predictive ARIMA framework strengthens planning by offering early warnings for heat risks under projected warming, critical for megacities facing pressures from population growth and climate change (Rizwan *et al*., 2008).

The integration of LCZ in predictive models is particularly significant for global South contexts, where rapid vertical growth, unplanned sprawl, and infrastructural inequities intensify thermal exposure (Emmanuel & Krüger, 2012). Ultimately, this study shows that SUHII is not uniform but a spatially stratified risk that can be systematically identified, forecast, and mitigated through advanced remote sensing and modelling. The observed seasonal variation in night-time SUHII across MMR reflects the combined effects of maritime influence, atmospheric stability, and surface characteristics. Winter shows stronger SUHII due to calm, dry conditions favouring heat retention, while summer convection and sea-breeze circulation enhance heat dissipation, reducing the urban–rural thermal contrast significantly. It sets a methodological benchmark for other rapidly urbanising regions, emphasising that daily-resolution, morphology-aware, and cloud-based analyses are essential for evidence-driven climate resilience in megacities.

CONCLUSIONS

The research addressed in the study revolved around three questions. The first aimed to observe whether SUHI existed in MMR. The answer indicates regions of exceptional temperature regimes, though trends are dissimilar. The analysis confirms that SUHII intensity in Mumbai is seasonally modulated, with pronounced winter heat retention and mitigated summer effects driven by stronger coastal ventilation. These findings emphasise the city's unique maritime thermal regulation, underscoring that urban planning must account for seasonal variations in boundary-layer dynamics to manage heat exposure and energy demand effectively.

While SUHI is generally expected to be positive, exceptions exist even in central metropolitan areas, though surroundings show enhanced SUHII. The nature and magnitude of SUHI vary seasonally more than geographically. Interestingly, the lower SUHII range in highly built-up regions requires exploration. It can be concluded that SUHI and SUHII require investigation from additional aspects, as direct correlations are primarily observed in LULC and particularly surface imperviousness.

Built-up and imperviousness correlate directly with SUHI but less with SUHII. Greater similarity is seen with LCZs, where open low-rise emerges as a major SUHI contributor without influencing intensity. The analysis is significant for detailed planning, with findings supporting future research in environment and climate change. Combining multiple parameters strengthens the study, enabling comparisons with other Indian cities. Given urbanisation's dynamism, such databases supplement limited field data, offering advantages of large-area coverage otherwise difficult in complex, fast-changing urban settings.

This study presents a nuanced, spatio-temporal assessment of SUHII in the Mumbai Metropolitan Region (MMR) over two decades (2003–2023), combining remote sensing data, geospatial sampling, and urban climatic zoning. By integrating LST with surface imperviousness (GHSL), LULC, and LCZ classifications, it captures both magnitude and spatial heterogeneity of urban heat phenomena. The analysis confirms a sustained urban–rural temperature gap of ~2 °C, with core city areas showing highest LST values—especially pre-monsoon peaks above 50 °C. ARIMA-based forecasting underscores a continued upward trend, highlighting the urgency for long-term mitigation. Yet, built-up density and SUHII are not linearly related; while imperviousness contributes, LCZ analysis shows urban morphology, locational factors and land-use function are stronger thermal predictors.

It is important to stress that SUHI and SUHII are not synonymous. SUHI denotes generally elevated urban surface temperatures, while SUHII refers to the intensity of the urban–rural contrast. These do not always align spatially or statistically. Areas may show high SUHI but

weak SUHII, particularly in coastal or vegetated zones. Recognising this distinction is vital for interpreting thermal dynamics. In conclusion, this study highlights MMR's complex and spatially heterogeneous urban heat patterns, shaped by land cover, surface characteristics, and form. The integrated use of GEE, LULC, LCZ, and statistical methods offers valuable insights for climate-sensitive urban planning.

The novelty lies in methodological blending—Earth observation, statistical modelling, and LCZs-driven zonal analysis. Exploratory use of deep learning improves pattern detection and spatial inference, particularly in classifying structures and understanding gradients across varied urban typologies. This comprehensive approach moves beyond urban–rural contrasts, showing how form, function, and materiality influence heat dynamics. The results are directly relevant to planners, policymakers, and designers working to reduce thermal risk with evidence-based strategies. Given MMR's scale, ecological vulnerability, and continued urban expansion, this analysis underscores the urgency of climate-sensitive planning—emphasising adaptive zoning, vegetation expansion, and thermally efficient infrastructure. As climate change intensifies urban heat stress, integrated approaches are critical to ensure liveability, equity, and resilience in megacities like Mumbai.

CONFLICT OF INTEREST

The author declares that there are no competing interests.

REFERENCES

Aayog (2021). *Reforms in urban planning capacity in India.* NITI Aayog.

Alexander, P.J., & Mills, G. (2014). Local climate classification and Dublin's urban heat island. *Atmosphere, 5*(4), 755–774. https://doi.org/10.3390/atmos5040755.

Alves, E., Anjos, M., & Galvani, E. (2020). Surface urban heat island in middle city: Spatial and temporal characteristics. *Urban Science, 4*(4), 54. https://doi.org/10.3390 /urbansci4040054.

Bechtel, B., Alexander, P.J., Böhner, J., Ching, J., Conrad, O., Feddema, J., Mills, G., See, L., & Stewart, I. (2019). Generating WUDAPT Level 0 data: Current status of production and evaluation. *Urban Climate, 27,* 24–45. https://doi.org/10.1016/j.uclim.2018.10.001.

Bhatia, S.Y., Patil, G.R., & Buddhiraju, K.M. (2023). Analysing urban sprawl of the Mumbai Metropolitan Region using remote sensing and socioeconomic data. *The International Archives of the Photogrammetry, Remote Sensing and Spatial Information Sciences, XLVIII-M-3*, 35–42. https://doi.org/10.5194/isprs-archives-XLVIII-M-3-2023-35-2023.

Budhiraja, B., Gawuc, L., & Agrawal, G. (2019). Seasonality of surface urban heat island in Delhi city region measured by local climate zones and conventional indicators. *IEEE Journal of Selected Topics in Applied Earth Observations and Remote Sensing, 12*(12), 5223–5232. https://doi.org/10.1109/jstars.2019.2955133.

Box, G.E.P., Jenkins, G.M., & Reinsel, G.C. (2015). *Time series analysis: Forecasting and control* (5th ed.). Wiley.

Census of India. (2011). *Population census 2011.* Government of India.

Cheval, S., Dumitrescu, A., Amihăesei, V., Irașoc, A., Paraschiv, M.G., & Ghent, D. (2023). A country scale assessment of the heat hazard-risk in urban areas. *Building and Environment, 229,* 109892. https://doi.org/10.1016/j.buildenv.2022.109892.

Cleveland, R.B., Cleveland, W.S., McRae, J.E., & Terpenning, I. (1990). STL: A seasonal-trend decomposition procedure based on loess. *Journal of Official Statistics*, 6(1), 3–73.

Derdouri, A., Wang, R., Murayama, Y., & Osaragi, T. (2021). Understanding the links between LULC changes and SUHI in cities: Insights from two-decadal studies (2001–2020). *Remote Sensing, 13*(18), 3654. https://doi.org/10.3390/rs13183654.

Dhar, T.K., & Khirfan, L. (2017). Climate change adaptation in the urban planning and design research: Missing links and research agenda. *Journal of Environmental Planning and Management, 60*(4), 602–627. https://doi.org/10.1080/09640568.2016.1178107.

Dihkan, M., Karsli, F., Guneroglu, A., & Guneroglu, N. (2015). Evaluation of surface urban heat island (SUHI) effect on coastal zone: The case of Istanbul megacity. *Ocean & Coastal Management, 118,* 309–316. https://doi.org/10.1016/j.ocecoaman.2015.03.008.

Dwivedi, A., & Khire, M.V. (2018). Application of split-window algorithm to study urban heat island effect in Mumbai through land surface temperature approach. *Sustainable Cities and Society, 41,* 865–877. https://doi.org/10.1016/j.scs.2018.02.030.

Dwivedi, A. (2019). Macro- and micro-level studies using urban heat islands to simulate effects of greening, building materials and other mitigating factors in Mumbai city. *Architectural Science Review, 62*(2), 126–144. https://doi.org/10.1080/00038628 .2019.1578193.

Emmanuel, R., & Krüger, E. (2012). Urban heat island and its impact on climate change resilience in a shrinking city: The case of Glasgow, UK. *Building and Environment, 53*, 137–149. https://doi.org/10.1016/j.buildenv.2012.01.020.

Fang, Q., Liu, C., Ren, Z., Fu, Y., Fan, H., Wang, Y., & Yu, Z. (2024). Spatiotemporal analysis of surface urban heat island dynamics in central Yunnan city cluster. *Sustainability, 16*(11), 4819. https://doi.org/10.3390/su16114819.

Gaur, A., Eichenbaum, M.K., & Simonovic, S.P. (2018). Analysis and modelling of surface urban heat island in 20 Canadian cities under climate and land-cover change. *Journal of Environmental Management, 206*, 145–157. https://doi.org/10.1016/j.jenvman.2017.10.002.

Gazi, A., & Mondal, I. (2018). Urban heat island and its effect on dwellers of Kolkata Metropolitan Area using geospatial techniques. *International Journal of Computer Sciences and Engineering, 6*(10), 741–753. 10.26438/ijcse/v6i10.741753.

Geletič, J., Lehnert, M., Savić, S., & Milošević, D. (2019). Inter-/intra-zonal seasonal variability of the surface urban heat island based on local climate zones in three central European cities. *Building and Environment, 156*, 21–32. https://doi.org/10.1016/ j.buildenv.2019.04.011.

González, Á. (2020). Influence of pavements on the urban heat island phenomenon: A scientific evolution analysis. *Energy and Buildings, 226*, 110379. https://doi.org/10.1016/ j.enbuild.2020.110379.

Gorelick, N., Hancher, M., Dixon, M., Ilyushchenko, S., Thau, D., & Moore, R. (2017). Google Earth Engine: Planetary-scale geospatial analysis for everyone. *Remote Sensing of Environment, 202*, 18–27. https://doi.org/10.1016/j.rse.2017.06.031.

Grover, A., & Singh, R.B. (2015). Analysis of urban heat island (UHI) in relation to Normalised Difference Vegetation Index (NDVI): A comparative study of Delhi and Mumbai. *Environments, 2*(2), 125–138. https://doi.org/10.3390/environments2020125.

Grover, A., & Singh, R.B. (2016). Monitoring spatial patterns of land surface temperature and urban heat island for sustainable megacity. *Journal of Environmental Research and Development, 7*(1), 38–54. https://doi.org/10.1177/0975425315619722.

Haashemi, S., Weng, Q., Darvishi, A., Kazem Alavipanah, S., Bechtel, B., Keramitsoglou, I., Kotthaus, S., Voogt, J.A., Zakšek, K., & Thenkabail, P. (2016). Seasonal variations of the surface urban heat island in a semi-arid city. *Remote Sensing, 8*(4), 352. https://doi.org/10.3390/rs8040352.

Hou, L., Yue, W., & Liu, X. (2021). Spatiotemporal patterns and drivers of summer heat island in Beijing-Tianjin-Hebei urban agglomeration, China. *IEEE Journal of Selected Topics in Applied Earth Observations and Remote Sensing, 14*, 7516–7527. https://doi.org/10.1109/JSTARS.2021.3094559.

Hsu, A., Sheriff, G., Chakraborty, T., & Manya, D. (2021). Disproportionate exposure to urban heat island intensity across major US cities. *Nature Communications, 12*(1), 1–11. https://doi.org/10.1038/s41467-021-22799-5.

Hulley, M.E. (2012). The urban heat island effect: Causes and potential solutions. In *Metropolitan Sustainability: Understanding and Improving the Urban Environment* (pp. 79–98). Woodhead Publishing. https://doi.org/10.1533/9780857096463.1.79.

Jain, M. (2023). Two decades of night-time surface urban heat island intensity analysis over nine major populated cities of India and implications for heat stress. *Frontiers in Sustainable Cities, 5*, 10. https://doi.org/10.3389/frsc.2023.1084573.

Kabisch, N., Korn, H., Stadler, J., & Bonn, A. (2017). Nature-based solutions to climate change adaptation in urban areas—Linkages between science, policy and practice. In N. Kabisch, H. Korn, J. Stadler, & A. Bonn (Eds.), *Nature-based solutions to climate change adaptation in urban areas: Theory and practice of urban sustainability transitions* (pp. 1–11). Springer, Cham. https://doi.org/10.1007/978-3-319-56091-5_1.

Kikon, N., Singh, P., Singh, S.K., & Vyas, A. (2016). Assessment of urban heat islands (UHI) of Noida City, India using multi-temporal satellite data. *Sustainable Cities and Society, 22*, 19–28. https://doi.org/10.1016/j.scs.2016.01.005.

Kim, H.H. (2007). Urban heat island. *International Journal of Remote Sensing, 13*(12), 2319–2336. https://doi.org/10.1080/01431169208904271.

Kotharkar, R., & Bagade, A. (2018). Evaluating urban heat island in the critical local climate zones of an Indian city. *Landscape and Urban Planning, 169*, 92–104. https://doi.org/10.1016/j.landurbplan.2017.08.009.

Kusak, L., & Kucukali, U.F. (2024). Investigating the relationship between COVID-19 shutdown and land surface temperature on the Anatolian side of Istanbul using large architectural impermeable surfaces. *Environment, Development and Sustainability, 26*, 18439–18476. https://doi.org/10.1007/s10668-023-03397-5.

Lau, K.K.L., Chung, S.C., & Ren, C. (2019). Outdoor thermal comfort in different urban settings of sub-tropical high-density cities: An approach of adopting local climate zone (LCZ) classification. *Building and Environment, 154*, 227–238. https://doi.org/10.1016/j.buildenv.2019.03.005.

Lazzarini, M., Marpu, P.R., & Ghedira, H. (2013). Temperature–land cover interactions: The inversion of urban heat island phenomenon in desert city areas. *Remote Sensing of Environment, 130*, 136–152. https://doi.org/10.1016/j.rse.2012.11.007.

Li, H., Zhou, Y., Li, X., Meng, L., Wang, X., Wu, S., & Sodoudi, S. (2018). A new method to quantify surface urban heat island intensity. *Science of the Total Environment, 624*, 262–272. https://doi.org/10.1016/j.scitotenv.2017.11.360.

Lin, P., Lau, S.S.Y., Qin, H., & Gou, Z. (2017). Effects of urban planning indicators on urban heat island: A case study of pocket parks in high-rise high-density environment. *Landscape and Urban Planning, 168*, 48–60. https://doi.org/10.1016/j.landurbplan.2017.09.024.

Lu, Y., Wu, P., Ma, X., Yang, H., & Wu, Y. (2020). Monitoring seasonal and diurnal surface urban heat islands variations using Landsat-scale data in Hefei, China, 2000–2017. *IEEE Journal of Selected Topics in Applied Earth Observations and Remote Sensing, 13*, 6410–6423. https://doi.org/10.1109/JSTARS.2020.3035040.

Maral, S.G., & Mukhopadhyay, T. (2015). Signal of urban heat island (UHI) effect: A case study of Mumbai Metropolitan Region. *Mausam, 66*(4), 729–740. https://doi.org/10.54302/mausam.v66i4.580.

Martilli, A., Krayenhoff, E.S., & Nazarian, N. (2020). Is the urban heat island intensity relevant for heat mitigation studies? *Urban Climate, 31*, 100541. https://doi.org/10.1016/j.uclim.2019.100541.

Kumar, R., & Mishra, V. (2019). Decline in surface urban heat island intensity in India during heatwaves. *Environmental Research Communications, 1*(3), 031001. https://doi.org/10.1088/2515-7620/ab121d.

Mumbai Metropolitan Region Development Authority (MMRDA). (2021). *Mumbai Metropolitan Region Development Authority Annual Report 2020–21*. https://mmrda.maharashtra.gov.in.

Mumbai Metropolitan Region Development Authority (MMRDA). (2023). *Final regional plan for Mumbai Metropolitan Region REF report (English)*. https://mmrda.maharashtra.gov.in/documents/10180/21354726/Final+Regional+Plan+for+Mumbai+Metropolitan+Region+REF+Report+%28English%29/bb3af422-5e0c-4790-8872-00b8f8b2479.

Morabito, M., Crisci, A., Guerri, G., Messeri, A., Congedo, L., & Munafò, M. (2021). Surface urban heat islands in Italian metropolitan cities: Tree cover and impervious surface influences. *Science of the Total Environment, 751*, 142334. https://doi.org/10.1016/j.scitotenv.2020.142334.

Nayak, S., Vinod, A., & Prasad, A.K. (2023). Spatial characteristics and temporal trend of urban heat island effect over major cities in India using long-term space-based MODIS land surface temperature observations (2000–2023). *Applied Sciences, 13*(24), 13323. https://doi.org/10.3390/app132413323.

Oke, T.R. (1995). The heat island of the urban boundary layer: Characteristics, causes and effects. In *Wind climate in cities* (pp. 81–107). Springer. https://doi.org/10.1007/978-94-017-3686-2_5.

Pakarnseree, R., Chunkao, K., & Bualert, S. (2018). Physical characteristics of Bangkok and its urban heat island phenomenon. *Building and Environment, 143*, 561–569. https://doi.org/10.1016/j.buildenv.2018.07.042.

Qin, Y. (2015). A review on the development of cool pavements to mitigate urban heat island effect. *Renewable and Sustainable Energy Reviews, 52*, 445–459. https://doi.org/10.1016/j.rser.2015.07.177.

Qin, Y., McVicar, T.R., Huang, J., West, S., & Steven, A. (2022). On the validity of using ground-based observations to validate geostationary-satellite-derived direct and diffuse surface solar irradiance: Quantifying the spatial mismatch and temporal averaging issues. *Remote Sensing of Environment, 280*, 113179. https://doi.org/10.1016/j.rse.2022.113179.

Quang, N.H., Quinn, C.H., Carrie, R., Stringer, L.C., Hue, L.T.V., Hackney, C.R., & Tan, D.V. (2022). Comparisons of regression and machine learning methods for estimating mangrove above-ground biomass using multiple remote sensing data in the Red River Estuaries of Vietnam. *Remote Sensing Applications: Society and Environment*, 26**,** 100725. https://doi.org/10.1016/j.rsase.2022.100725.

Rasul, A., Balzter, H., Smith, C., Remedios, J., Adamu, B., Sobrino, J.A., Srivanit, M., & Weng, Q. (2017). A review on remote sensing of urban heat and cool islands. *Land, 6*(2), 38. https://doi.org/10.3390/land6020038.

Ren, J., Wang, W., Wei, J., Li, H., Li, X., Liu, G., Chen, Y., & Ye, S. (2023). *Evolution and prediction of drought-flood abrupt alternation events in Huang-Huai-Hai River Basin, China*. Science of the Total Environment, 869, 161707. https://doi.org/10.1016/j.scitotenv.2023.161707.

Rizwan, A.M., Dennis, L.Y.C., & Liu, C. (2008). A review on the generation, determination and mitigation of urban heat island. *Journal of Environmental Sciences, 20*(1), 120–128. https://doi.org/10.1016/S1001-0742(08)60019-4.

Sachindra, D.A., Ng, A.W.M., Muthukumaran, S., & Perera, B.J.C. (2016). Impact of climate change on urban heat island effect and extreme temperatures: A case-study. *Quarterly Journal of the Royal Meteorological Society, 142*(694), 172–186. https://doi.org/10.1002/qj.2642.

Sahu, S., & Saizen, I. (2018). Development of planning index for evaluating climate change protocols: Analysis of Mumbai Metropolitan Region's Regional Plan 1996–2011. *City, Territory and Architecture, 5*(1), 5. https://doi.org/10.1186/s40410-018-0082-8.

Santamouris, M. (2020). Recent progress on urban overheating and heat island research. Integrated assessment of the energy, environmental, vulnerability and health impact. *Energy and Buildings, 207,* 109482. https://doi.org/10.1016/j.enbuild.2019.109482.

Sarif, M.O., Rimal, B., & Stork, N.E. (2020). Assessment of changes in land use/land cover and land surface temperatures and their impact on surface urban heat island phenomena in the Kathmandu Valley (1988–2018). *ISPRS International Journal of Geo-Information, 9*(12), 726. https://doi.org/10.3390/ijgi9120726.

Shahfahad, Talukdar, S., Rihan, M., Hang, H.T., Bhaskaran, S., & Rahman, A. (2022). Modelling urban heat island (UHI) and thermal field variation and their relationship with land use indices over Delhi and Mumbai metro cities. *Environment, Development and Sustainability, 24*(3), 3762–3790. https://doi.org/10.1007/s10668-021-01587-7.

Sharma, R., Chakraborty, A., & Joshi, P.K. (2015). Geospatial quantification and analysis of environmental changes in urbanizing city of Kolkata (India). *Environmental Monitoring and Assessment*, 187(1), Article 4206. https://doi.org/10.1007/s10661-014-4206-7.

Shaw, A. (2012). Urbanisation and environmental challenges in Mumbai. *Cities*, 29(2), 142–149.

Stewart, I.A., & Oke, T.R. (2012). Local climate zones for urban temperature studies. *Bulletin of the American Meteorological Society, 93*(12). https://doi.org/10.1175/BAMS-D-11-00019.1.

Stewart, I.A., & Mills, G. (2021). *The urban heat island: A guidebook*. Elsevier.

Su, Y., Wu, J., Zhang, C., Wu, X., Li, Q., Liu, L., Bi, C., Zhang, H., Lafortezza, R., & Chen, X. (2022). Estimating the cooling effect magnitude of urban vegetation in different climate zones using multi-source remote sensing. *Urban Climate, 43*, 101155. https://doi.org/10.1016/j.uclim.2022.101155.

Swain, D., Roberts, G.J., Dash, J., Lekshmi, K., Vinoj, V., & Tripathy, S. (2017). Impact of rapid urbanisation on the city of Bhubaneswar, India. *Proceedings of the National Academy of Sciences India Section A - Physical Sciences, 87*(4), 845–853. https://doi.org/10.1007/s40010-017-0453-7.

Thomas, G., Sherin, A.P., Ansar, S., & Zachariah, E.J. (2014). Analysis of urban heat island in Kochi, India, using a modified local climate zone classification. *Procedia Environmental Sciences, 21*, 3–13. https://doi.org/10.1016/j.proenv.2014.09.002.

Tran, H., Uchihama, D., Ochi, S., & Yasuoka, Y. (2006). Assessment with satellite data of the urban heat island effects in Asian mega cities. *International Journal of Applied Earth Observation and Geoinformation*, 8(1), 34–48. https://doi.org/10.1016/j.jag.2005.05.003.

Veena, K., Parammasivam, K. M., & Venkatesh, T. N. (2020). Urban heat island studies: Current status in India and a comparison with international studies. *Journal of Earth System Science, 129*(1), 1–15. https://doi.org/10.1007/s12040-020-1351-y.

Voogt, J.A. (2020). Urban heat islands. In Y. Wang (Ed.), *Atmosphere and climate*. CRC Press.

Voogt, J.A., & Oke, T.R. (2003). Thermal remote sensing of urban climates. *Remote Sensing of Environment*, 86(3), 370–384. https://doi.org/10.1016/S0034-4257(03)00079-8.

UN-Habitat. (2022). *World Cities Report 2022: Envisaging the future of cities*. United Nations Human Settlements Programme.

Veena, K., Parammasivam, K.M., & Venkatesh, T.N. (2020). Urban heat island studies: Current status in India and a comparison with international studies. *Journal of Earth System Science, 129*(1), 1–15. https://doi.org/10.1007/s12040-020-1351-y.

Vujovic, S., Haddad, B., Karaky, H., Sebaibi, N., & Boutouil, M. (2021). Urban Heat Island: Causes, Consequences, and Mitigation Measures with Emphasis on Reflective and Permeable Pavements. *Civil Engineering*, 2(2), 459–484. https://doi.org/10.3390/civileng 2020026 (mdpi.com).

Zhao, C., Yu, B., & Chen, Z. (2022). Deep learning for urban climate mapping using satellite time-series. *ISPRS Journal of Photogrammetry and Remote Sensing, 188*, 220–233. https://doi.org/10.1016/j.isprsjprs.2022.02.012.

Zhou, D., Xiao, J., Bonafoni, S., Berger, C., Deilami, K., Zhou, Y., Frolking, S., Yao, R., Qiao, Z., & Sobrino, J.A. (2018). Satellite remote sensing of surface urban heat islands: Progress, challenges, and perspectives. *Remote Sensing, 11*(1), 48. https://doi.org/10.3390/rs11010048.

Zhou, X., & Chen, H. (2018). Impact of urbanisation-related land use land cover changes and urban morphology changes on the urban heat island phenomenon. *Science of the Total Environment, 635*, 1467–1476. https://doi.org/10.1016/j.scitotenv.2018.04.091.

Zhou, D., Zhao, S., Zhang, L., Sun, G., & Liu, Y. (2021). The footprint of urban heat island effect in China's 32 major cities: Spatiotemporal patterns and associated drivers. *Remote Sensing of Environment, 265*, 112682. https://doi.org/10.1016/j.rse.2021.112682.

Zhou, Y., Zhao, H., Mao, S., Zhang, G., Jin, Y., Luo, Y., Huo, W., Pan, Z., An, P., & Lun, F. (2022). Exploring surface urban heat island (SUHI) intensity and its implications based on urban 3D neighbourhood metrics: An investigation of 57 Chinese cities. *Science of the Total Environment, 847*, 157662. https://doi.org/10.1016/j.scitotenv.2022.157662.